공학석사 학위논문

Fluorinated Phenylene Unit as a Building Block for High Performance *n*-Type Semiconducting Polymer

Fluorinated Phenylene을 사용한 높은 성능의

n형 유기 고분자 반도체

2013년 2월

서울대학교 대학원

재료공학부

박 정 하

↑
2cm
↓

Fluorinated Phenylene Unit as a Building Block for High Performance *n*-Type Semiconducting Polymer

2013년

↑
2.5cm
↓

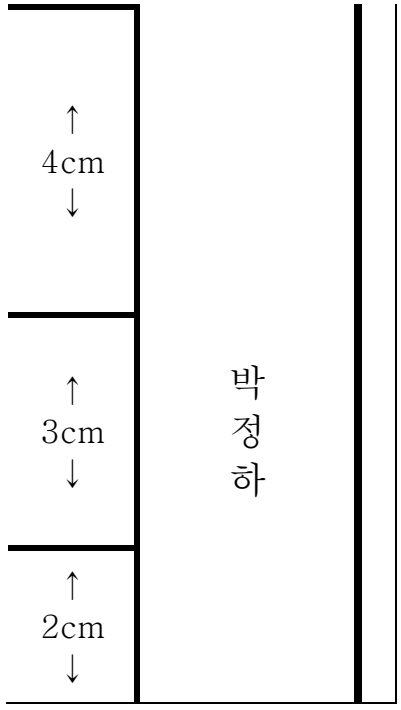
↑
4cm
↓
↑
3cm
↓
↑
2cm
↓
박
정
하

Fluorinated Phenylene Unit as a Building Block for High Performance *n*-Type Semiconducting Polymer

지도 교수 조 원 호

이 논문을 공학석사 학위논문으로 제출함
2012년 12월

서울대학교 대학원
재료공학부
박 정 하

박정하의 석사 학위논문을 인준함
2012년 12월

위 원 장 김장주 (인)

부위원장 조원호 (인)

위 원 박수영 (인)

Abstract

Fluorinated Phenylene Unit as a Building Block for High Performance *n*-Type Semiconducting Polymer

Park, Jung Ha

Department of Materials Science and Engineering

Seoul National University

Intense research efforts have been devoted to the development of *p*-type semiconducting polymers for OFETs due to their synthetic accessibility, whereas *n*-type polymer semiconductors have been scarcely reported, although realization of air-stable and solution-processable *n*-channel polymers is important to the function of *p*-*n* junction diode, organic photovoltaics, and complementary organic circuits. Herein, we report the synthesis and *n*-channel transporting property of copolymers composed of diketopyrrolopyrrole unit and fluorinated phenyl unit, where the number of fluorine substitution varies. When the effect of the number of fluorine substitution on the *n*-channel transporting property is examined, it reveals that the polymer with four fluorine substitution exhibits the best *n*-type charge transporting behavior with an electron mobility of 1.71 $cm^2 \cdot V^{-1} \cdot s^{-1}$.

Keywords: Organic field-effect transistor, *n*-type organic semiconductor, fluorinated phenylene, diketopyrrolopyrrole

Student Number: 2011-22862

Contents

List of Schemes

List of Figures

List of Tables

.

Chapter 1. Introduction

Numerous semiconducting materials showing promising electronic properties for organic electronics have been developed in recent years.[1,2] Semiconducting polymers are particularly attractive because they could be readily processed in solution with high quality film formation and therefore printable in large-area electronic circuits on flexible substrates with low fabrication cost.[3] Hence semiconducting polymers have frequently been used in OFETs as either *p*-channel or *n*-channel materials.[4-6] Recently, remarkable progress in the performance of OFETs based on semiconducting polymers has been achieved as a result of development in material design/synthesis and morphology/device optimization. One of promising approaches for high OFET performance is to use a donor–acceptor (D–A) type alternating copolymer composed of electron rich and electron deficient units. The introduction of the D–A structure into a polymer backbone induces intermolecular charge transport, leading to an increased molecular ordering through the self-assembly of rigid backbone of semiconducting polymer and thus to an improved charge carrier mobility. Also, the D–A strategy for designing semiconducting polymers have been very effective to tune the molecular energy level including the highest occupied molecular orbital (HOMO) and the

lowest unoccupied molecular orbital (LUMO) energy levels and hence alter the charge transport characteristics in OFETs.

An impressive progress in developing *p*-channel semiconducting polymers has recently been made due to their synthetic accessibility and relatively high air-stability. Current state-of-the-art charge carrier mobility of semiconducting polymer is close to 10 $cm^2 \cdot V^{-1} \cdot s^{-1}$ for *p*-channel operation, which is comparable to the amorphous Si-based FETs while high performance *n*-channel semiconducting polymers for OFETs have scarcely been reported, although efficient *n*-channel conduction in organic materials is crucial to function of $p-n$ junction diodes, organic photovoltaics, and complementary organic circuits. Especially organic complementary circuits are currently at an early stage of development because of the scarcity of ambient stable and high performance *n*-channel organic semiconductors.[7]

Recently, it has been reported that rational molecular design of semiconducting polymers incorporating strong electron-withdrawing groups such as halogens,[8] cyano,[9] or diimide moieties[10] onto chain backbone, can afford promising *n*-channel semiconducting polymers for OFETs, where electron-withdrawing groups pull electrons out of π-conjugated backbone and then lower the frontier energy levels. Among electron withdrawing groups, fluorine atom has unique properties such as the highest Pauling electronegativity of 4.0 and the small atom size (van der Waals radius, r=1.35 Å, only slightly larger than hydrogen, r=1.2 Å), and thus the fluorine substitution may not cause steric

hindrance to the molecular packing of fluorine-substituted polymers.[11-13] Also, due to strong electronegativity of fluorine, the fluorination of organic semiconductors lowers not only the HOMO energy level which enhances the oxidative stability, but also the LUMO energy level facilitating easier electron injection from electrode in OFET device. Interestingly, it has been reported that the fluorination of organic semiconductors can alter the polarity of charge carrier transport from *p*-type, ambipolar, to solely *n*-type in OFETs.[14] Moreover, the interaction C–F---H–C in fluorinated organic compounds may induce the self-organization and crystallization, which may enhance the charge carrier mobility of organic semiconductors.[15] Until now, the fluorination of oligomers has been successfully developed for synthesis of semiconductors, while the fluorination of polymers for *n*-type semiconductors has not been explored,[16-19] although fluorine-substituted D–A semiconducting polymers have recently been developed for their applications in organic photovoltaics with successful fine-tuning of the energy levels.[20] Therefore, it is expected that fluorination of conjugated polymers alters the polarity of charge carrier transport and therefore can be used for developing high performance *n*-type semiconducting polymers for OFETs.

One of the promising building blocks for high mobility semiconducting polymer is diketopyrrolopyrrole (DPP). Very recently, D–A copolymers based on DPP have emerged as an active material for OFETs due to its planar structure capable of forming π–π stacks in the

solid state leading to efficient charge transport. Hence, copolymerization of DPP with electron donating monomers have shown to afford semiconducting copolymers exhibiting high *p*-channel or balanced ambipolar charge transport behavior.[21-24] However, the DPP-based semiconducting polymers have not exhibited satisfactory electron-transporting property for *n*-channel operation. Here, we report alternating D–A copolymers composed of DPP and fluorinated phenyl unit where the number of fluorine substitution on phenylene varies from one to four for OFET application. As the number of fluorine substitution increases, the charge transport in OFETs changes from predominant *p*-type, balanced ambipolar, to superior *n*-type behavior. Consequently, the copolymer with four fluorine substitution exhibits high *n*-type charge transport with an electron mobility of 1.71 $cm^2 \cdot V^{-1} \cdot s^{-1}$.

Chapter 2. Experimental

2.1 Materials

1,4-Dibromo-2-fluorobenzene, 1,4-dibromo-2,5-difluorobenzene, and 1,4-dibromo-tetrafluorobenzene were purchased from Tokyo Chemical Industry (TCI). 1,4-Benzenediboronic acid bis(pinacol) ester (compound **2**) was purchased from Sigma-Aldrich Chemical Co..

2.2 Synthesis of monomers

2.2.1 Synthesis of 1-Fluoro-2,5-di(4ʾ,4ʾ,5ʾ,5ʾ-tetramethyl [1ʾ,3ʾ,2ʾ] dioxaborolan -2ʾ-yl)benzene. (3)

1,4-dibromo-2-fluorobenzene (500 mg, 1.969 mmol), pinacoldiboron ester (1065 mg, 4.19 mmol), and KOAc (579 mg, 5.9 mmol) in DMF solution (5 mL) were charged in microwave reactor vial. The mixture was purged for 20 min and $PdCl_2$(dppf) (42 mg, 0.053 mmol) was added at last. The mixture was heated at 160 ℃ for 2 h in microwave reactor, and subsequently cooled. The product was extracted with brine and dicholoromethane, and dried over $MgSO_4$. After solvent was evaporated under reduced pressure, the crude product was purified by

column chromatography in hexane. The pure white crystals of the product were obtained from recrystallization of the solid from hexane. (160 mg, 23% yield)

^{1}H NMR (300 MHz, CDCl3, δ): 7.70 (t, 1H), 7.53 (d, 1H), 7,43 (d, 1H), 1.35(s, 24H).

^{13}C NMR (500 MHz, $CDCl_3$, δ): 24.81, 84.29, 122.25, 122.36, 122.40, 122.52, 161.45, 161.49, 163.44, 163.48. HRMS (EI+) *m*/*z*: 348.5, 349 (calcd for $C_{18}H_{27}B_2FO_4$ (MH+) 348.2).

2.2.2 Synthesis of 1,4-Difluoro-2,5-di(4',4',5',5'-tetramethyl[1',3',2'] dioxaborolan-2'-yl)benzene. (4)

1,4-dibromo-2,5-difluorobenzene (2 g, 7.36 mmol), pinacoldiboron ester (3.98 g, 0.0157 mol), and KOAc (3.15 g, 0.032 mol) in DMF solution (5 mL) were charged in microwave reactor vial. The mixture was purged for 20 min and $PdCl_2$(dppf) (112 mg, 0.153 mmol) was added at last. The mixture was heated at 160 ℃ for 2 h in microwave reactor, and subsequently cooled. The product was extracted with brine, H_2O, and dichloromethane; dried over $MgSO_4$. After solvent was evaporated under reduced pressure, the crude product was purified by column chromatography. The pure white crystals of the product were obtained from recrystallization of the solid from hexane. (580 mg, 22% yield)

^{1}H NMR (300 MHz, $CDCl_3$, δ): 7.33 (t, 2 H, J = 6.6 Hz), 1.35 (s, 24 H).

^{13}C NMR (500 MHz, $CDCl_3$, δ): 24.81, 84.29, 122.25, 122.36, 122.40, 122.52, 161.45, 161.49, 163.44, 163.48. HRMS (EI+) *m*/*z*: 366.3 (calcd for $C_{18}H_{27}B_2F_2O_4$ (MH+) 366.2).

2.2.3 Synthesis of 2,3,5,6-tetrafluoro-1,4-phenylene (bis(triemethyltin)) (5)

n-BuLi (2.5M in hexane, 6.39 ml, 10.227 mmol) was added dropwise to a solution of 1,4-dibromotetrafluorobenzene (1.5 g, 4.87 mmol) in ahydrous tetrahydrofuran (30 mL) at −78℃ under an argon atmosphere and the mixture was stirred for 1 h. To the stirred solution, trimethyltin chloride (1.0M in THF, 10.23 ml, 10.227 mmol) was added at −78℃ and the reaction mixture was stirred overnight at room temperature. The solution was poured into water and the organic layer was extracted with diethyl ether; solvent was removed to give a white solid. Recrystallization from petroleum ether gave white solid crystals. (690 mg, 30% yield)

^{13}C NMR (500 MHz, $CDCl_3$, δ): –9.23, –9.16, –7.72, –6.28, 6.21, 0.02, 147.17, 147.23, 147.29, 147.35, 147.38, 147.40, 147.50, 149.12, 149.22, 149.25, 149.30, 149.33, 149.41, 149.45. HRMS (EI+) *m*/*z*: 478, 463, 461(calcd for $C_{18}H_{24}B_2F_4O_4$ (MH+) 477.9).

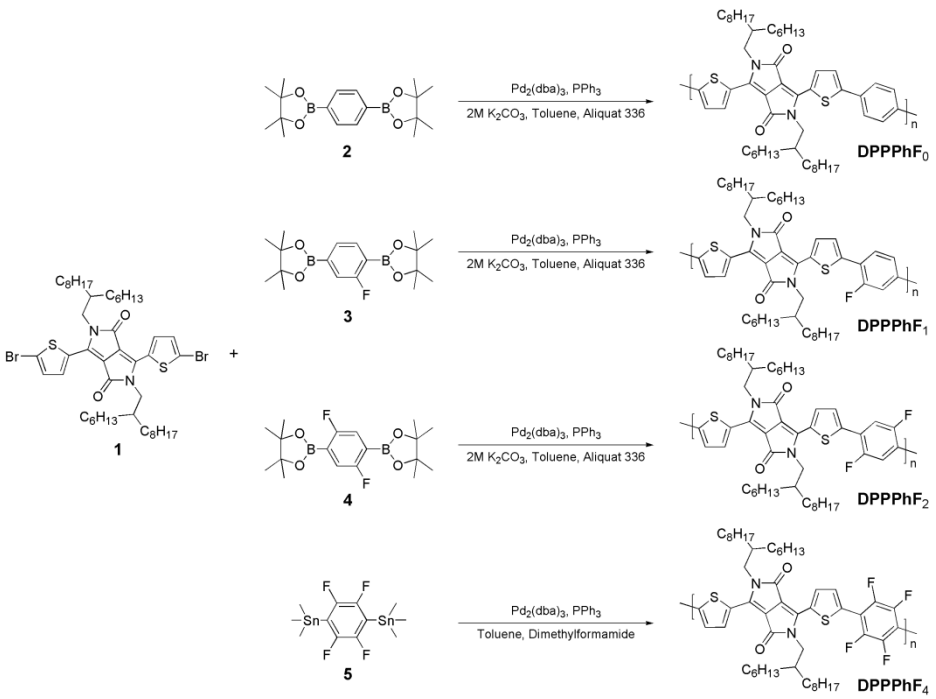

Scheme 2.1 Synthesis of conjugated polymers containing fluorinated phenyl units.

2.3 Synthesis of polymers

DPP-based semiconducting polymers, $DPPPhF_0$, $DPPPhF_1$, and $DPPPhF_2$, were synthesized via the Suzuki coupling between dibrominated thiophene-end capped DPP (**1**) and diboronated phenylene derivatives (**2, 3, 4**), and the $DPPPhF_4$ was synthesized via the Stille polycondensation reaction between **1** and distannyl-tetrafluorophenylene (**5**) (Scheme 2.1).

2.3.1 Synthesis of $DPPPhF_0$

Tris(dibenzylideneacetone)dipalladium (10 mg, 11 μmol) was added to a mixture of 3,6-bis(5-bromo-2-thienyl)-2,5-dihydro-2,5-di(2-hexyldecyl)-pyrrolo[3,4c]pyrrolo-1,4-dione (221 mg, 244 μmol), 1,4-di-(4,4,5,5-tetramethyl-1,3-dioxaboralane)-benzene (80.5 mg, 244 μmol), in toluene (4.5 mL), triphenylphosphine (7 mg, 26 μmol), and K_2CO_3 (143.74 mg, 1.04 mmol) in demineralised water (0.5 mL). This mixture was stirred for 3 days at 150 ℃ in in microwave reactor after which the crude polymer was precipitated in methanol. The precipitate was collected in a Soxhlet thimble and was extracted with methanol, acetone, hexane, and chloroform until the extracts were colorless. The chloroform fraction was reduced in volume and precipitated in methanol and filtered over a 4.5 μm PTFE filter. The polymer was

collected and dried in a vacuum oven at 60 ℃ overnight, resulting in 141 mg (69%) of a dark powder.

2.3.2 Synthesis of $DPPPhF_1$

Tris(dibenzylideneacetone)dipalladium(0) ($Pd_2(dba)_3$, 11.8 mg, 0.0129 mmol) was added to an argon bubble mixture of 3,6-bis(5-bromo-2-thienyl)-2,5-dihydro-2,5-di(2-hexyldecyl)-pyrrolo[3,4c]pyrrolo-1,4-dione (260 mg, 0.287 mmol), compound **3** (100 mg, 0.287 mmol), 2 drops of aliquot 336, triphenyl phosphine (PPh_3, 8.02 mg, 0.031 mmol), and 2 M solution of potassium carbonate (K_2CO_3) in 0.5 ml of degassed water in toluene (4 mL) with degassed water (0.5 mL). This mixture was stirred for 3 h at 160℃ in microwave reactor after which the crude polymer was precipitated in methanol. The precipitate was collected in a Soxhlet thimble and was extracted with methanol, acetone, ethyl acetate, hexane, and chloroform until the extracts were colorless. The chloroform solution was concentrated and reprecipitated in methanol; filtered and dried under vacuum. (169 mg, 70% yield)

2.3.3 Synthesis of $DPPPhF_2$

To a solution of 3,6-bis(5-bromo-2-thienyl)-2,5-dihydro-2,5-di(2-hexyldecyl)pyrrolo [3,4c]pyrrolo-1,4-dione (247 mg, 0.273 mmol), compound **4** (100 mg, 0.273 mmol), and triphenyl phosphine (PPh_3,

7.63 mg, 0.0291 mmol) in toluene (4.5 ml), 2 M solution of potassium carbonate (K_2CO_3) in 0.5 ml of degassed water was added. Then, 2 drops of aliquot 336 was added to this solution and purged for 20 min. At last, $Pd_2(dba)_3$ (11.27 mg, 0.0123 mmol) was added. The mixture was stirred for 3 h at 160℃ in microwave reactor. The crude polymer was precipitated in methanol and then soxhlet extracted with methanol, acetone, ethyl acetate, hexane, and chloroform until the extracts were colorless. The chloroform solution was concentrated and reprecipitated in methanol; filtered and dried under vacuum. (142 mg, 60% yield)

2.3.4 Synthesis of DPPPhF$_4$

Compound **5** (100 mg, 0.209 mmol), 3,6-bis(5-bromo-2-thienyl)-2,5-dihydro-2,5-di(2-hexyldecyl)pyrrolo [3,4c]pyrrolo-1,4-dione (189.21 mg, 0.209 mmol), and PPh_3 (7.63 mg, 0.0291 mmol) in toluene (5 ml) and DMF (1 ml) solution are purged for 20 min. $Pd_2(DBA)_3$ (5.9 mg, 0.0221 mmol) was added finally, and the mixture was stirred for 3 h at 160℃ in microwave reactor. Similar procedures described for **DPPPhF$_2$** were followed afterwards. (118 mg, 63% yield)

2.4 Characterization

The chemical structures were identified by ^{1}H NMR (Avance DPX-300) and ^{13}C NMR (Avance DPX-500). Elemental analyses were recorded with a Jeol JMS600w in fast atom bombardment mode. Molecular weight (M_n) and its polydispersity index (PDI) of all synthesized polymers were determined by GPC (Knauer K-501 pump with a K-2301 refractive index detector) running in chloroform, calibrated with narrow polydispersity polystyrene standards. Thermogravimetric analysis (TGA) was carried out using a thermogravimetric analyzer (TA 2050) at a heating rate of 10 ℃ min^{-1} under nitrogen atmosphere. The UV-visible absorption spectra were recorded on a Perkin-Elmer Lambda 25 spectrometer.

Cyclic voltammetry were conducted on a potentiostat/galvanostat (VMP 3, Biologic) in an electrolyte solution of 0.1 M tetrabutylammonium hexafluorophosphate in acenonitrile. Pt wires (Bioanalytical System Inc.) were used as both counter and working electrodes, and silver/silver ion (Ag in 0.1 M $AgNO_3$ solution, Bioanalytical System Inc.) was used as a reference electrode. Grazing-incidence X-ray diffraction measurements were performed at the Pohang Accelerator Laboratory. The measurements were obtained with a scanning interval of 2º between 3º and 32º.

2.5 Device Fabrication and Characterization.

Bottom-contact top-gate OFETs were fabricated using heavily doped Si wafer as the bottom gate electrode with 300 nm of SiO_2 layer as the gate dielectric. Gold source and drain electrodes (40 nm) were patterned by the vacuum evaporation. The substrate was cleaned in acetone and isopropanol, and dried in an oven at 130 ℃. The device was treated with UV ozone for 0.5 h, and then the SiO_2 layer was treated with ODTS for 2 h by vacuum evaporation in an oven at 80 ℃. The device was rinsed and sonicated with toluene, and dried in an oven at 150 ℃. The polymers were dissolved in chloroform at a concentration of 4 mg mL^{-1} by stirring for two days. The polymer films were spin-cast at 3000 rpm and dried at 60 ℃ for 0.5 h, and annealed at a designated temperature for 0.5 h. Finally, the 40 nm thick gold top contact was thermally evaporated in vacuum through a shadow mask with a channel width of 1500 μm and a length of 200 μm. The field effect mobilities were extracted from the saturation regime using the relationship $\mu_{sat}=(2I_{DS}L)/(WC(V_G-V_{th})^2)$, where I_{DS} denotes the saturation drain current, C is the capacitance ($C_i = 10.8 \times 10^{-9}$ F·cm^{-2}) of SiO_2 dielectric, V_G is the gate bias, and V_{th} is the threshold voltage. OFETs were characterized under nitrogen atmosphere using Keitheley 4200 and MST5000A.

Chapter 3. Results and Discussion

3.1 Synthesis and Characterization

The chemical structures of 1-fluoro-2,5-di(4',4',5',5'-tetramethyl [1',3',2']dioxaborolan-2'-yl)benzene (3), 1,4-Difluoro-2,5-di(4',4',5',5'-tetramethyl[1',3',2']dioxaborolan-2'-yl)benzene (4), and 2,3,5,6-tetrafluoro-1,4-phenylene(bis(triemethyltin)) (5) are identified by ^{1}H NMR as shown in Figure 3.1–3.3, repectively. The number-average molecular weight with narrow molecular weight distribution of $DPPPhF_0$, $DPPPhF_1$, $DPPPhF_2$, and $DPPPhF_4$ are determined by GPC as shown in Table 3.1.

3.2 Electrochemical properties

When the ionization potentials of four polymers were measured in thin film by cyclic voltammetry (CV) (Table 3.1 and Figure 3.4), $DPPPhF_0$ without fluorine substitution exhibits the HOMO level of –5.36 eV and the LUMO level of –3.56 eV. Furthermore, the substitution of the electron-withdrawing fluorine significantly lowers the HOMO level of the polymers: the HOMO levels of $DPPPhF_1$, $DPPPhF_2$, and $DPPPhF_4$ are –5.45 eV, –5.57 eV, and –5.65 eV, respectively, while the LUMO

levels of $DPPPhF_1$ and $DPPPhF_2$ do not change significantly. However, when the LUMO levels are calculated by subtracting the optical bandgaps from the HOMO levels, as measured by CV, the LUMO energy level also decreases with the increasing fluorine content. Among four polymers, $DPPPhF_4$ has the lowest LUMO level of –4.18 eV, indicating that the charge injection from the electrode to the semiconducting polymer becomes effective due to the largely reduced electron injection barrier.

3.3 Optical properties

When the UV-visible absorption spectra of four polymers in chloroform solution and in solid film are compared, as shown in Figure 3.5, the four polymers exhibit nearly the same spectra, indicating that the fluorine substitution does not affect the conformation and molecular arrangement of chain backbone. All polymers in film exhibited a red-shift of absorption by ~10 nm as compared to the absorption in solution due to polymer chain packing in the solid state.

3.4 Calculated dipole moments of the polymers

When the dipole moments of repeating units of $DPPPhF_0$ and $DPPPhF_4$ are calculated, the values of $DPPPhF_0$ and $DPPPhF_4$ are 0.79 D and

1.68 D with opposite direction, respectively, (Figure 3.6) indicating that the fluorinated phenylene unit becomes stronger accepting unit than DPP. Moreover, the torsional angles between thiophene and phenylene ring in $DPPPhF_0$ and $DPPPhF_4$ are 18.36° and 8.50°, respectively, which are much smaller than the limiting value 30° for coplanarity to achieve intramolecular π overlap enough to generate an efficient conduction band.[25] Since $DPPPhF_4$ has smaller torsional angle than the $DPPPhF_0$, it is expected that $DPPPh_4$ has better coplanarity for π–π stacking and therefore exhibits better charge transport.

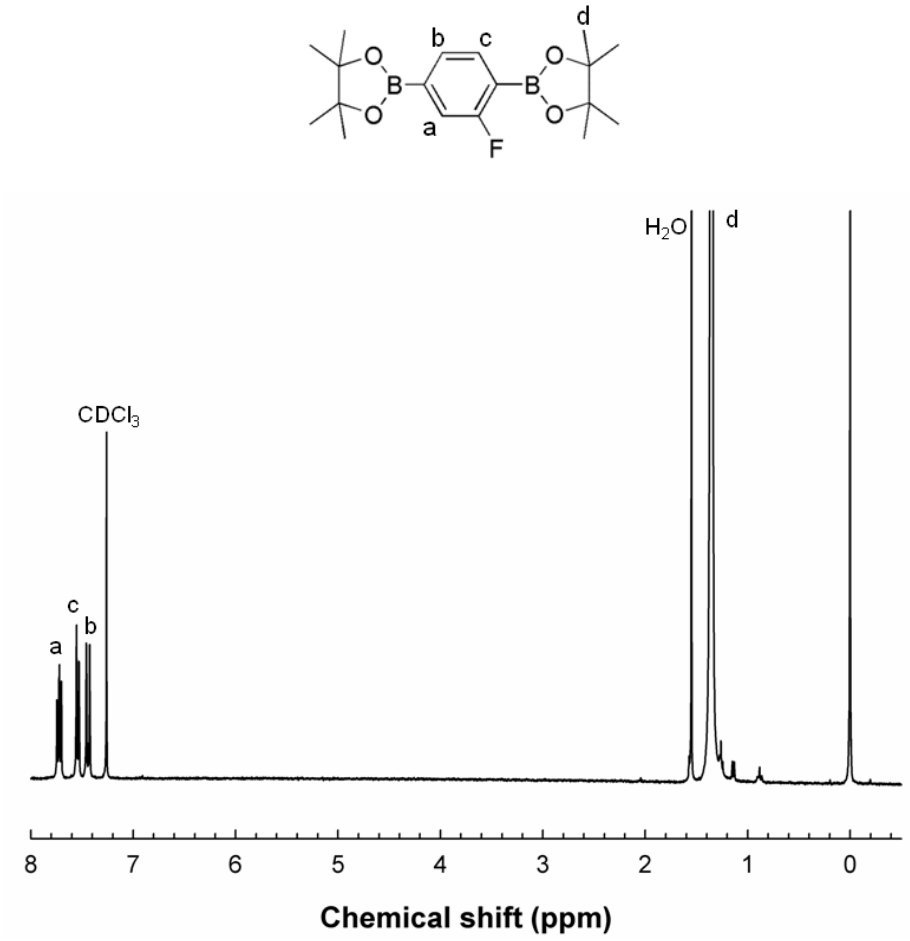

Figure 3.1 Chemical structure of ^{1}H NMR spectrum of **3**

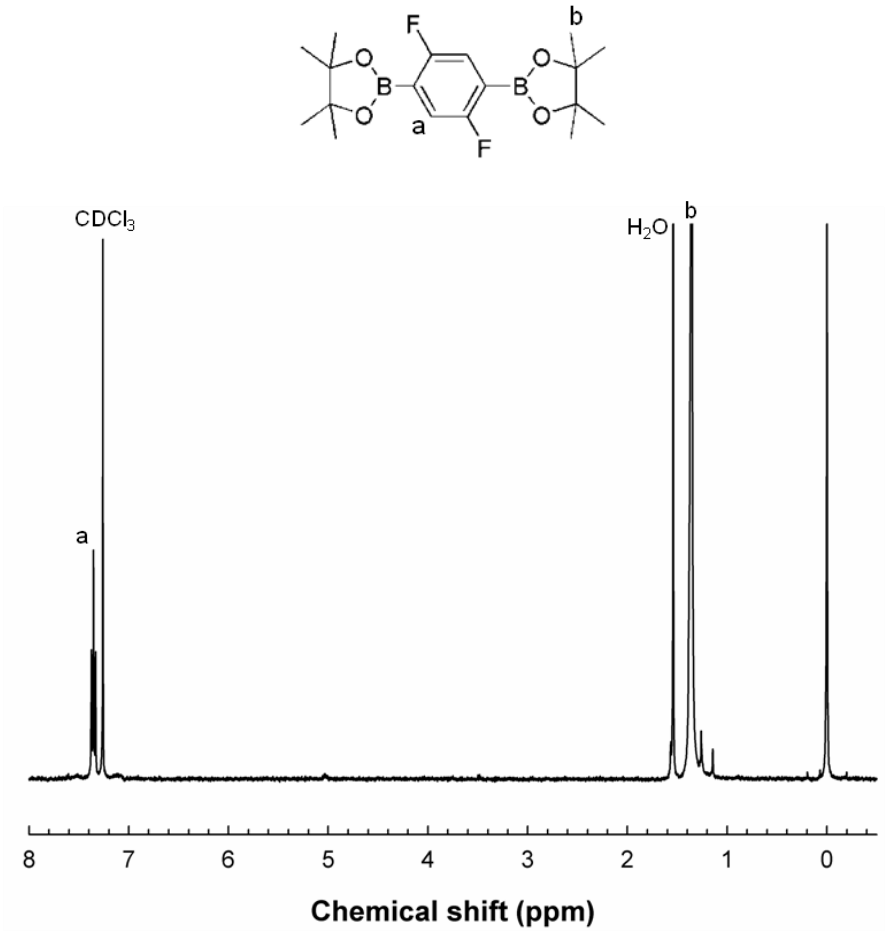

Figure 3.2 Chemical structure of ^{1}H NMR spectrum of **4**

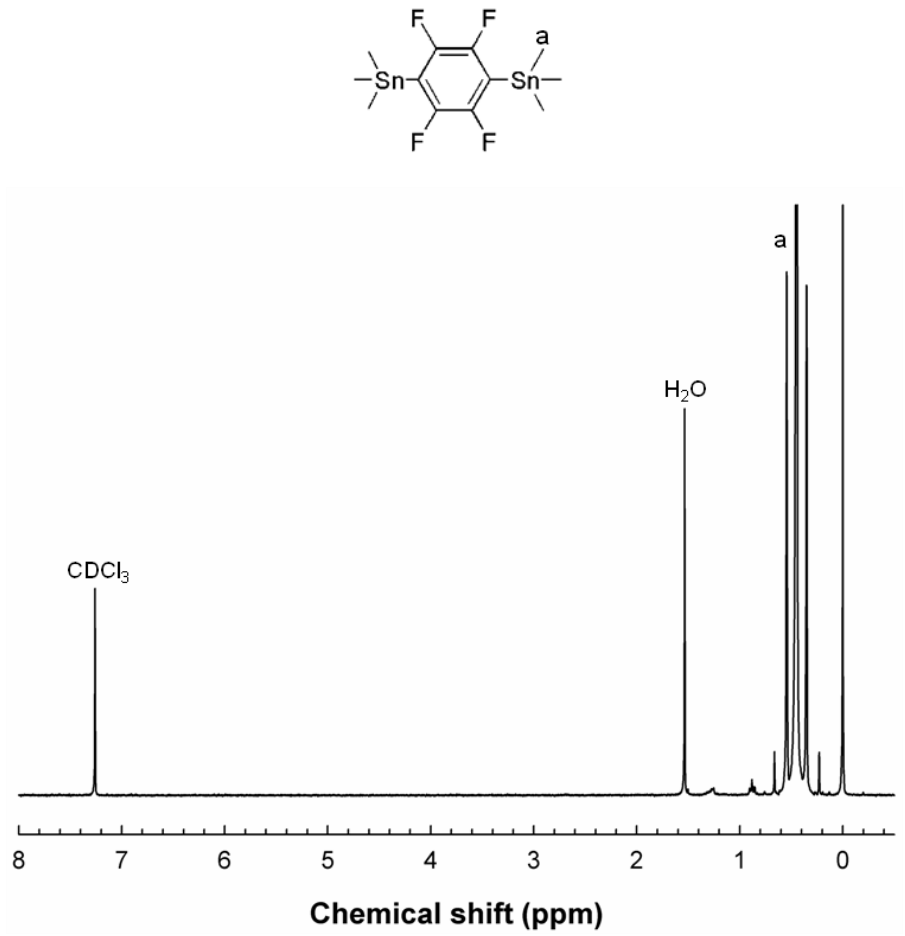

Figure 3.3 Chemical structure of ^{1}H NMR spectrum of **5**

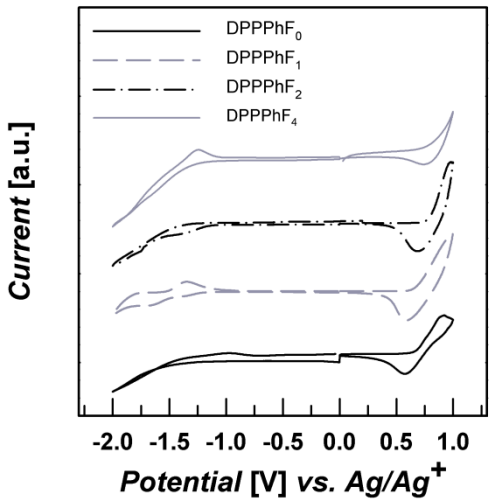

Figure 3.4 Cyclic voltammograms of polymers

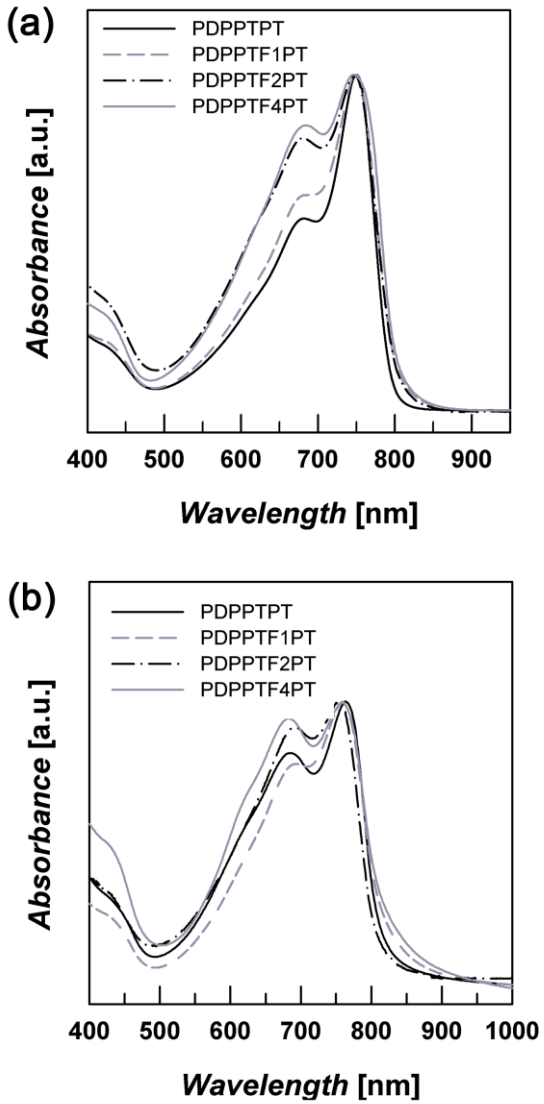

Figure 3.5 UV-vis absorption spectrum of the polymers in $CHCl_3$ solution (a) and film (b)

Table 3.1 Characteristics of the polymers

Polymer	M_n [kg mol^{-1}]	PDI	E_g^{opt} [eV]	HOMO [eV]	LUMO [eV]	LUMO[a] [eV]
DPPPhF$_0$	17.4	2.01	1.50	–5.36	–3.56	–3.86
DPPPhF$_1$	54.0	1.94	1.49	–5.45	–3.57	–3.96
DPPPhF$_2$	18.8	1.73	1.52	–5.57	–3.56	–4.05
DPPPhF$_4$	16.3	1.79	1.47	–5.65	–3.64	–4.18

[a] Calculated from the optical bandgap and the HOMO level. LUMO = HOMO + E_g^{opt}

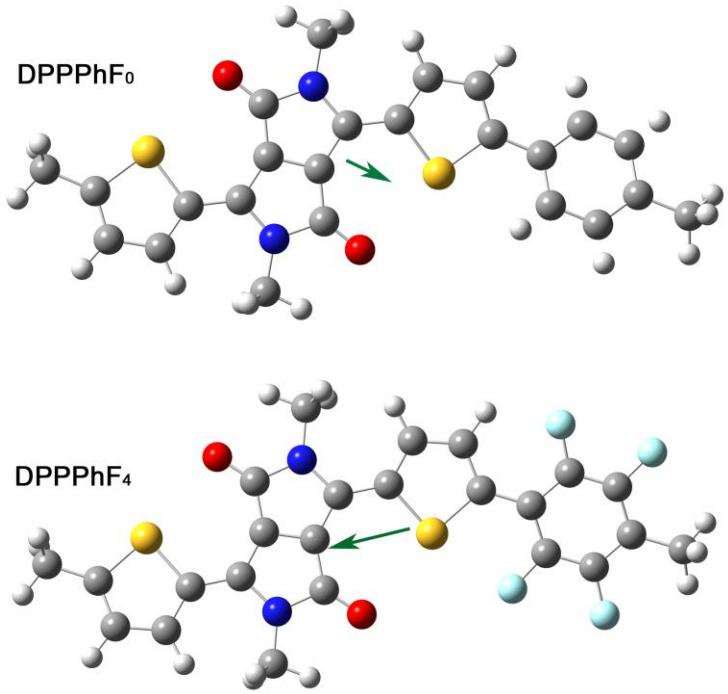

Figure 3.6 Calculated dipole moments of the polymers. Dipole moments of repeating units of $DPPPhF_0$ and $DPPPhF_4$ are calculated with TD-DFT B3LYP/6-31. The values of $DPPPhF_0$ and $DPPPhF_4$ are 0.79 D and 1.68 D with opposite direction, respectively, indicating that the fluorinated phenylene unit becomes even stronger accepting unit than DPP.

3.5 Organic field effect transistors performances

The charge transport properties of the semiconducting polymers were investigated using bottom-gate/top-contact transistor configuration with gold source/drain electrodes, where heavily *n*-doped silicon and SiO_2 are used as the gate electrode and the gate dielectric (capacitance C_i = 10.8×10^{-9} F·cm^{-2}), respectively. The SiO_2 dielectric was treated with octadecyltrichlorosilane (ODTS) prior to deposition of semiconducting polymer to both passivate the SiO_2 surface and enhance the ordering of polymer at the dielectric interface. The four different semiconducting polymers, were subsequently deposited by spin coating of dilute chloroform solutions. The device was annealed at various temperatures to optimize the device performance. The performances are summarized in Table 3.2 (Figure 3.7–3.11).

The charge carrier mobilities of all four polymers increase as the annealing temperature increases up to 200 ℃. DPPPhF$_0$ and DPPPhF$_1$ have the best performance when annealed at 200 ℃, showing clear ambipolar transport behavior, while DPPPhF$_2$ and DPPPhF$_4$ have the best performance after annealing at 250 ℃ and 280 ℃, respectively, showing *n*-type dominant transistor behavior.

Since DPPPhF$_4$ has the lowest LUMO level as determined by CV, it is expected that DPPPhF$_4$ exhibits *n*-type charge transport behavior. As shown in Figure 3.11, the output and transfer characteristics of an

OFET device with $DPPPhF_4$ thin film annealed at 280 ℃ reveals the highest electron mobility of 1.71 $cm^2 \cdot V^{-1} \cdot s^{-1}$, indicating that more fluorine substitution on phenylene ring makes the polymer to have more *n*-channel transporting property. A moderate hole transport behavior is also observed owing to good match of the HOMO energy level (–5.65 eV) of $DPPPhF_4$ with the work function of gold. However, the hole transport is observed at a very low current in the *p*-channel operation mode, indicating that $DPPPhF_4$ is predominantly an electron transport semiconductor. This is probably because the substitution of strong electron-withdrawing fluorine atoms lowers the LUMO energy level of $DPPPhF_4$ and thus reduces the electron injection barrier from the gold electrode to the polymer, facilitating effectively electron transport. As the number of fluorine substitution increases, the charge transport behavior changes from *p*-type to *n*-type transistor (Table 3.2). This result clearly demonstrates that the low LUMO energy level is necessary to facilitate electron transport.

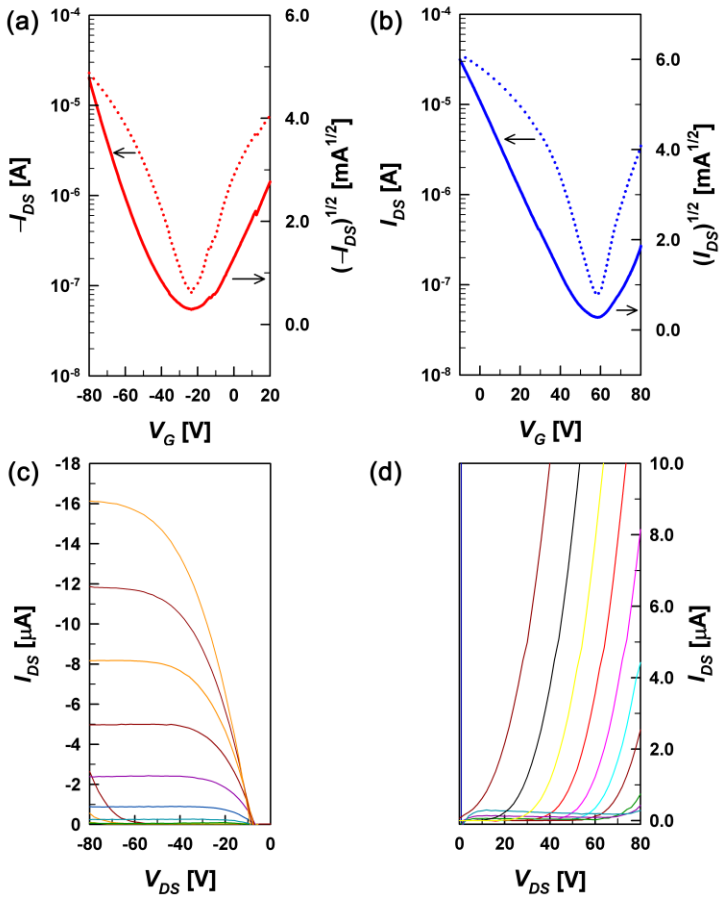

Figure 3.7 Performance of an transistor based on DPPPhF$_0$ annealed at 200 °C. (**a**,**b**) OFET transfer plots of current versus V_G at negative source-drain bias (**a**) and at positive source-drain bias (**b**). (**c**,**d**) Current-voltage output plot as a function of V_G at negative source-drain bias (**c**) and at positive source-drain bias (**d**).

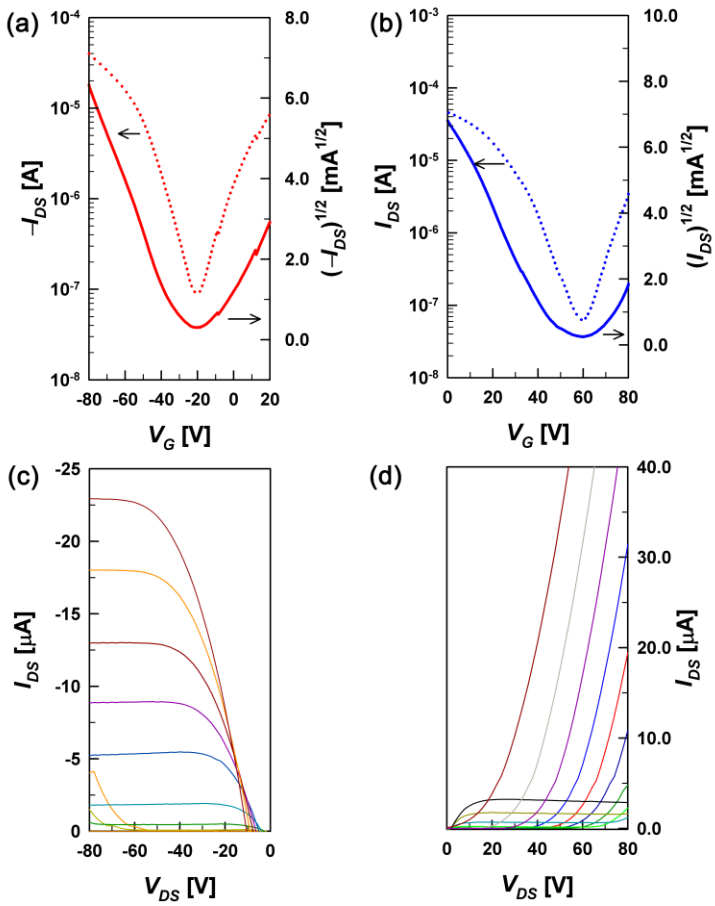

Figure 3.8 Performance of an transistor based on DPPPhF$_1$ annealed at 200 °C. (**a**,**b**) OFET transfer plots of current versus V_G at negative source-drain bias (**a**) and at positive source-drain bias (**b**). (**c**,**d**) Current-voltage output plot as a function of V_G at negative source-drain bias (**c**) and at positive source-drain bias (**d**).

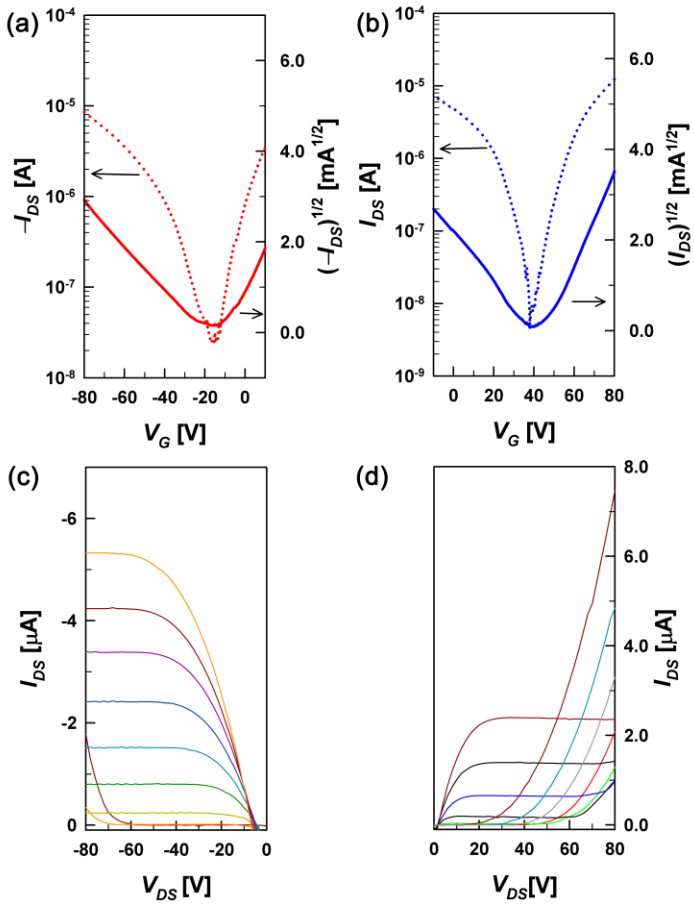

Figure 3.9 Performance of an transistor based on DPPPhF$_2$ annealed at 250 °C. (**a**,**b**) OFET transfer plots of current versus V_G at negative source-drain bias (**a**) and at positive source-drain bias (**b**). (**c**,**d**) Current-voltage output plot as a function of V_G at negative source-drain bias (**c**) and at positive source-drain bias (**d**).

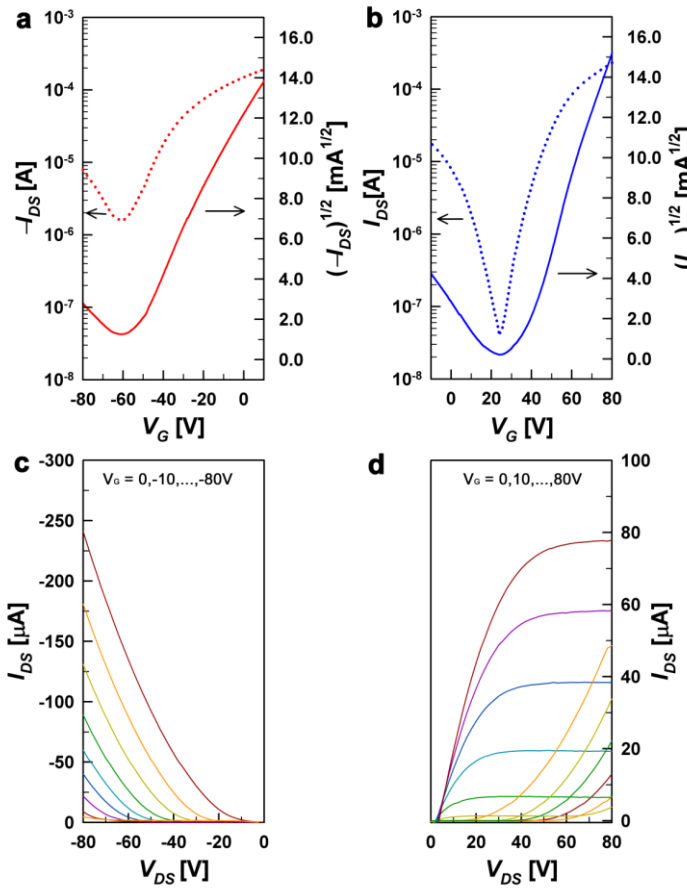

Figure 3.10 Performance of an transistor based on DPPPhF$_4$ annealed at 250 °C. (**a**,**b)** OFET transfer curves of current versus gate voltage (V_G) at negative source-drain bias (**a**) and at positive source-drain bias (**b**). The dotted lines represent transfer curves as a function of $|I_{DS}|$. The solid lines represent transfer curves as a function of $(I_{DS})^{1/2}$. (**c**,**d)** Current-voltage output curves as a function of V_G at negative source-drain bias (**c**) and at positive source-drain bias (**d**). Gate voltages were applied, changing from 0 to –80V in steps of –10V for (c) and 0 to 80V in steps of 10V for (d).

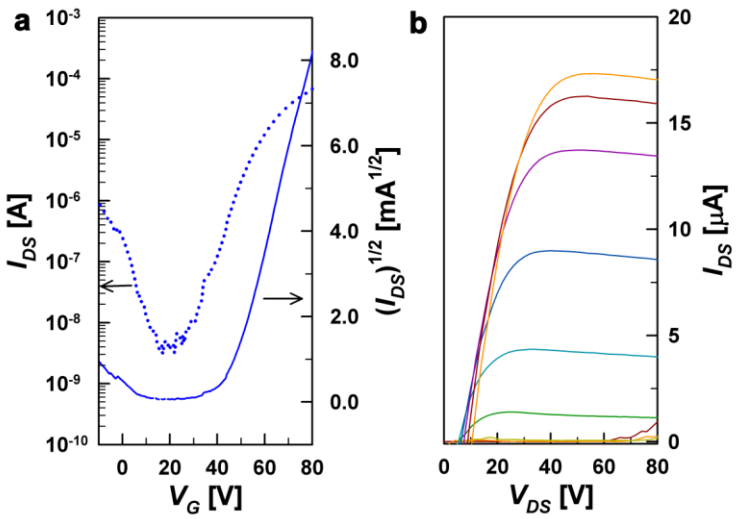

Figure 3.11 Performance of an transistor based on DPPPhF$_4$ annealed at 280 °C. (**a**) OFET transfer plots of current versus V_G at positive source-drain bias. The dotted lines represent transfer curves as a function of $|I_{DS}|$. The solid lines represent transfer curves as a function of $(I_{DS})^{1/2}$. (**b**) Current-voltage output plot as a function of V_G at positive source-drain bias. Gate voltages were applied, changing from 0 to 80V in steps of 10V.

Table 3.2 Summary of the device properties of the polymer-based

OFETs as a function of annealing temperature.

Polymer	Annealing temperature	μ_h ($cm^2 V^{-1} s^{-1}$)	μ_e ($cm^2 V^{-1} s^{-1}$)
DPPPhF$_0$	100 ℃	0.064	-
	200 ℃	0.30	0.23
	250 ℃	0.12	0.079
DPPPhF$_1$	100 ℃	0.060	0.00123
	200 ℃	0.30	0.26
	250 ℃	0.225	0.001
DPPPhF$_2$	100 ℃	0.031	0.07
	200 ℃	0.02	0.09
	250 ℃	0.03	0.123
	280 ℃	0.03	0.08
DPPPhF$_4$	100 ℃	0.017	0.49
	200 ℃	0.14	0.81
	250 ℃	0.19	1.35
	280 ℃	0.20	1.71
	300 ℃	-	1.05

3.6 Molecular orientation

To further understand the transport property as observed above, we investigated the change in the microstructure of the four polymers upon annealing using 2D grazing-incidence wide-angle X-ray scattering (GIWAXS) (Figure 3.12). The GIWAXS data of as-spun films of all four polymers reveal weak orders of alkyl stacking (h00) peaks along the q_z axis (the out-of-plane direction), indicating that the crystalline domains have preferentially edge-on orientation on the substrate. Moreover, $DPPPhF_4$ show an additional peak at $q_z \sim 1.6$ $Å^{-1}$, corresponding to the (010) peak in out-of-plane direction, manifesting the existence of face-on orientation. All the 200 ℃ annealed films exhibited stronger and sharper diffraction peaks than as-cast films, indicating that thermal annealing increases crystallization. Since $DPPPhF_4$ shows sharper π–π stacking reflection than $DPPPhF_2$ in out-of-plane direction, $DPPPhF_4$ has more face-on orientation of crystallites than $DPPPhF_2$. When $DPPPhF_2$ and $DPPPhF_4$ are annealed at 250 ℃ and 280 ℃, respectively, the GIWAXS patterns show more clearly that $DPPPhF_4$ crystallites have both the face-on and edge-on molecular orientation on the substrate, while $DPPPhF_2$ crystallites have predominantly edge-on orientation (Figure 3.13). Considering that most organic materials with high charge carrier mobility exhibit preferentially edge-on packing on the substrate,[26, 27] it seems unusual that $DPPPhF_4$ showing both face-on and edge-on orientations has the highest *n*-type mobility. It has generally accepted that the edge-on packing of polymer molecules is advantageous and necessary for high

performance FETs due to edge-on charge transport along the chain backbone as well as the π–π stacking direction, whereas the face-on packing is considered inherently detrimental causing the poor device performance.[28-30] However, high mobility polymers have recently been developed, where the orientation of polymer backbones does not require orthogonal to the substrate.[31-33] For instance, poly{[N,N9-bis(2-octyldodecyl)-naphthalene-1,4,5,8-bis(dicarboximide)-2,6-diyl]-alt-5,59-(2,29-bithiophene)} (P(NDI2OD-T2) shows high electron mobility, but exhibits an exceptional degree of in-plane ordering and adopts largely the face-on packing, where the charge transports through subsequent layers coupled with the out-of-plane π-stacking.[33,34] Thus, it is expected that the face-on packing of $DPPPhF_4$ may also contribute the charge transport because $DPPPhF_4$ has both the face-on and edge-on packing texture. $DPPPhF_4$ is the most effective for charge transport through the edge-on orientation because the π–π stacking distance (d_{010}) of 200℃ annealed polymer film decreases from 4.08 Å to 3.93 Å as the number of fluorine substitution increases. Furthermore, the π–π stacking spacing of 280 ℃ annealed $DPPPhF_4$ film is 3.85 Å, which corresponds to the optimal intermolecular distance[35] for charge hopping with a preferred orientation of polymer backbone orthogonal to the substrate. When the coherence length (L_c) is determined from the full-width-at-half-maximum of x-ray reflection, the Scherrer equation, the L_c values of $DPPPhF_0$, $DPPPhF_1$, $DPPPhF_2$, and $DPPPhF_4$ are 39.7 Å, 42.5 Å, 26.6 Å, and 61.4 Å, respectively (Table 3.3). Since the

coherence length is related to the crystalline size and lattice order,[36] larger L_c has less grain boundaries and therefore renders better charge transport.[37,38] Since $DPPPhF_4$ has the largest coherence length of 61.4 Å, this also contributes to the highest *n*-type mobility. It is noteworthy that the smallest coherence length of $DPPPhF_2$ has the lowest charge mobility.

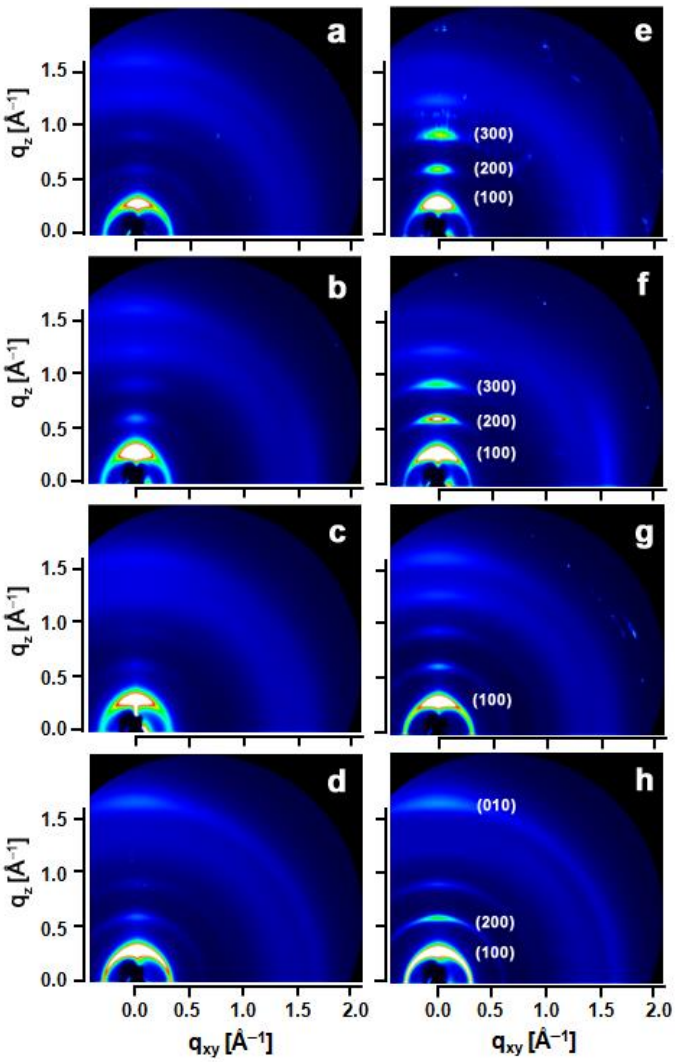

Figure 3.12 X-ray characterization of polymers from as-cast and 200 °C annealed films. Polymer films were deposited on SiO_2/SAM layers for XRD characterization. (**a-d**) 2D grazing incidence diffraction patterns of as-cast films of (**a**) $DPPPhF_0$, (**b**) $DPPPhF_1$, (**c**) $DPPPhF_2$ and (**d**) $DPPPhF_4$. (**e-h**) 2D GIXD images of 200 ℃ annealed films, (**e**) $DPPPhF_0$, (**f**) $DPPPhF_1$, (**g**) $DPPPhF_2$, and (**h**) $DPPPhF_4$.

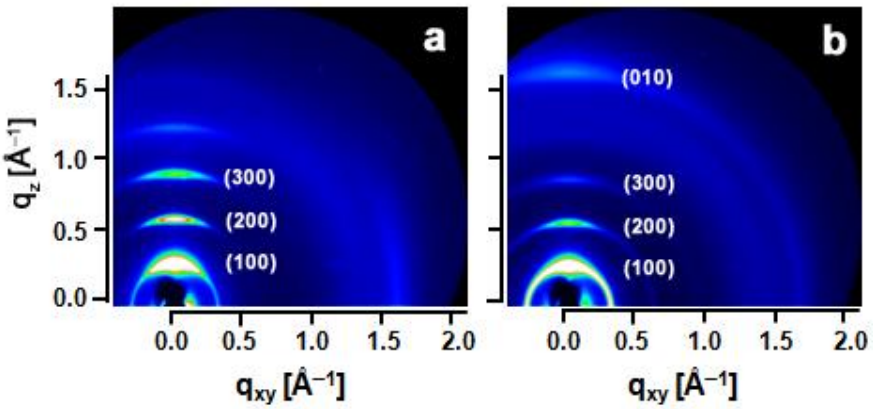

Figure 3.13 Comparison of X-ray diffraction pattern of $DPPPhF_2$ with $DPPPhF_4$. (**a**) 2D-GIXD image of $DPPPhF_2$ film annealed at 250 ℃. (**b**) 2D-GIXD image of $DPPPhF_4$ film annealed at 280 ℃. $DPPPhF_2$ crystallites have only (100), (200), and (300) peaks, indicating predominantly edge-on orientation, whereas $DPPPhF_4$ crystallites have additional (010) peak in out-of-plane direction, indicating that the crystallites have both the face-on and edge-on molecular orientation exists on the substrate.

Table 3.3 π–π stacking spacing (d_{010}) and coherence length determined from the in-plane scattering for all polymer films after annealing.

Annealing temperature	**DPPPhF$_0$**		**DPPPhF$_1$**		**DPPPhF$_2$**		**DPPPhF$_4$**	
	d_{010} (Å)	L_c (Å)	d_{010} (Å)	L_c (Å)	d_{010} (Å)	L_c (Å)	d_{010} (Å)	L_c (Å)
200 ℃	3.93	**39.69**	3.93	**42.54**	3.93	**26.62**	3.93	**61.4**

3.7 Discussions

Although the reason why four fluorine substituted polymer has the highest electron mobility is not fully understood, we suggest the following possibilities for the high mobility of $DPPPhF_4$. First, it has been known that donor-acceptor type alternating copolymers containing electron withdrawing groups such as benzothiazole, imide, and diketopyrrolopyrrole have dipoles oriented normal to the polymer backbone axis, which affords the optimal configuration for charge hopping due to dipole-dipole interaction.[35] Hence, the strong dipole moment of $DPPPhF_4$ induces strong dipole-dipole interaction to drive local ordering of chains and to orient adjacent backbones in an optimal conformation for effective charge hopping. Secondly, since it has also been reported that the face-on molecular orientation facilitates face-on charge transport through subsequent layers coupled with the out-of-plane π-stacking,[39–42] $DPPPhF_4$ with face-on orientation is expected to show high electron mobility. Previous studies[33,34] also demonstrated that P(NDI2OD-T2) showed the face-on orientation on the substrate, which facilitates efficient electron injection from gold electrode and low contract resistance, and as a result exhibited high electron mobility. Although it has been reported that the edge-on molecular packing is beneficial for several polymer FETs, the above finding clearly demonstrates that the face-on packing enhances the electron mobility.

Therefore, both the face-on and edge-on packings of $DPPPhF_4$ contribute to the high electron mobility, as schematically shown in Figure 3.14.

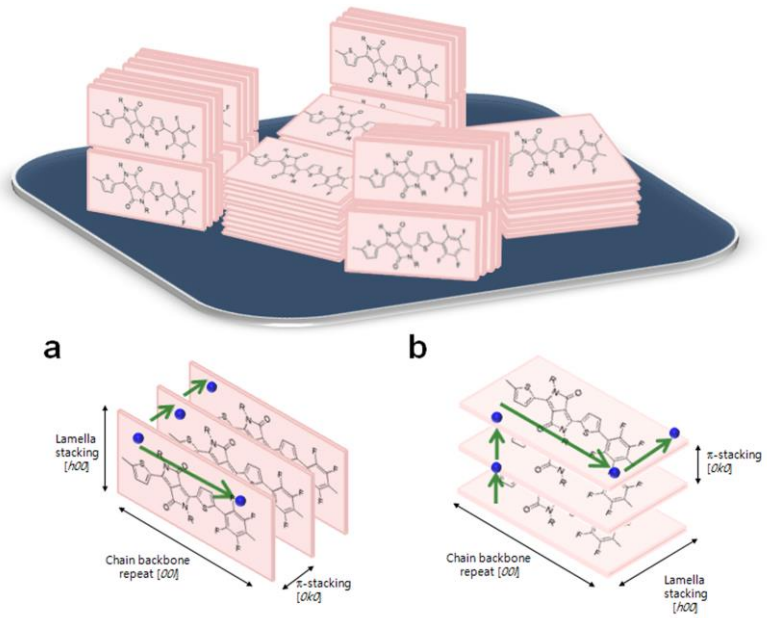

Figure 3.14 Schematic representation of charge carrier transport of $DPPPhF_4$ through edge-on and face-on orientation. The schematic **(a)** indicates the proposed microstructral arrangement in edge-on arrangement (out-of-plane orientation) on the substrate. The charge carrier (blue circles) hops to subsequent layers coupled by π-stacking and travels along the polymer backbone. The schematic **(b)** shows the proposed molecular orientation of face-on arrangement (in-plane orientation) in the substrate, where the charge carrier not only travels through chain axis, but also hops through lamella stacking direction.

Chapter 4. Conclusion

We have synthesized a series of donor-acceptor type conjugated polymers consisting of DPP and phenylene with different number of fluorine substitution to investigate the effect of fluorine substitution on the energy level, the crystal structure and charge carrier transport of the polymers. As the number of fluorine substitution increases, the LUMO energy level of the polymer becomes lower, the face-on orientation becomes favorable, and thereby the charge transporting behavior changes from *p*-type transistor to *n*-type transistor. Consequently, the polymer with four fluorine substitution, DPPPhF_4, exhibits *n*-type charge transporting behavior with an electron mobility of 1.71 $cm^2 \cdot V^{-1} \cdot s^{-1}$. This high electron mobility may arise from unique structural and electrochemical properties of the polymer, i.e., the lower LUMO energy level, the existence of both the edge-on and face-on orientation on the substrate, higher crystallinity, longer coherence length along the chain backbone and strong dipole moment of chain backbone to effectively induce charge hopping.

Bibliography

(1) Usta, H.; Facchetti, A.; Marks, T. J. *J. Am. Chem. Soc.* **2008**, *130*, 8580.

(2) Guo, X.; Ortiz, R. P.; Zheng, Y.; Hu, Y.; Noh, Y.; Baeg, K.; Facchetti, A.; Marks, T. J. *J. Am. Chem. Soc.* **2011**, *133*, 1405.

(3) Smith, J.; Hamilton, R.; McCulloch, I.; Stingelin-Stutzmann, N.; Heeney, M.; Bradley, D. D. C.; Anthopoulos, T. D. *J. Mater. Chem.* **2010**, *20*, 2562.

(4) Yan, H.; Chen, Z.; Zheng, Y.; Newman, C.; Qunn, J.; Dotz, F.; Kastler, M.; Facchetti, A. *Nature* **2009**, *457*, 679.

(5) Li, Y.; Singh, S. P.; Sonar, P. *Adv. Mater.* **2010**, *22*, 4862.

(6) Zhang, W.; Smith, J.; Watkins, S. E.; Gysel, R.; McGehee, M.; Salleo, A.; Kirkpatrick, J.; Ashraf, S.; Anthopoulos, T.; Heeney, M.; McCulloch, I. *J. Am. Chem. Soc.* **2010**, *132*, 11437.

(7) Gao, X.; Di, C.-an.; Hu, Y.; Yang, X.; Fan, H.; Zhang, F.; Liu, Y.; Li, H.; Zhu, D. et al. *J. Am. Chem. Soc.* **2010**, *132*, 3697.

(8) Tang, M. L.; Bao, Z. *Chem. Mater.* **2011**, *23*, 446.

(9) Anthony, J. E. *Chem. Mater.* **2011**, *23*, 583.

(10) Ortiz, R. P.; Herrera, H.; Blanco, R.; Huang, H.; Facchetti, A.; Marks, T. J.; Zheng, Y.; Segura, J. L. *J. Am. Chem. Soc.*

2010, *132*, 8440.

(11) Wong, S.; Ma, H.; Jen, A. K.-Y.; Barto, R.; Frank, C. W. *Macromolecules* **2003**, *36*, 8001.

(12) Reichenbächer, K.; Süss, H. I.; Hulliger, J. *Chem. Soc. Rev.* **2005**, *34*, 22.

(13) Babudri, F.; Farinola, M.; Naso, F.; Ragni, R. *Chem. Commun.* **2007**, 1003.

(14) Bredas, J. L.; Heeger, A. J. *Chem. Phys. Lett*. **1994**, *217*, 507.

(15) Wang, Y.; Parkin, S. R.; Gierschner, J.; Watson, M. D. *Org. Lett.* **2008**, *10*, 3307.

(16) Lin. Y. Y.; Dodabalapur, A.; Sarpeshkar, R.; Bao, Z.; Li, W.; Baldwin, K.; Raju, V. R.; Katz, H. E. *Appl. Phys. Lett*. **1999**, *74*, 2714.

(17) Yoon, M.-H.; DiBenedetto, S. A.; Facchetti, A.; Marks, T. J. *J. Am. Chem. Soc.* **2005**, *127*, 1348.

(18) Facchetti, A.; Yoon, M. H.; Stern, C. L.; Katz, H. E.; Marks, T. J. *Angew. Chem. Int. Ed.* **2003**, *42*, 3900.

(19) Oh, J. H.; Suraru, S.; Lee, W. Y.; Könemann, M.; Höffken, H. W.; Röger, C.; Schmidt, R.; Chung, Y.; Chen, W. C.; Würthner, F.; Bao. Z. *Adv. Funct. Mater.* **2010**, *20*, 2148.

(20) Zhou, H.; Yang, L.; Stuart, A. C.; Price, S. C.; Liu, S.; You, W. *Angew. Chem. Int. Ed.* **2011**, *50*, 2995.

(21) Wienk, M. M.; Turbiez, M.; Gilot, J.; Janssen, R. A. *Adv.*

Mater. **2008**, *20*, 2556.

(22) Sonar. P.; Singh, S. P.; Li, Y.; Soh, M. S.; Dodabalapur, A. *Adv. Mater.* **2010**, *22*, 5409.

(23) Yuen, J. D.; Fan, J.; Seifter, J.; Lim, B.; Hufschmid, R.; Heeger, A. J.; Wudl, F. *J. Am. Chem. Soc.* **2011**, *133*, 20799.

(24) Kronemeijer A. J.; Gili, E.; Shahid, M.; Rivnay, J.; Salleo, A.; Heeney, M.; Sirringhaus, H. *Adv. Mater.* **2012**, *24*, 1558.

(25) McCullough, R. D. *Adv. Mater.* **1998**, *10*, 93.

(26) Chabinyc, M. L.; Toney, M. F.; Kline, R. J.; McCulloch, I.; Heeney, M. *J. Am. Chem. Soc.* **2009**, *129*, 3226.

(27) Jimison, L. H.; Salleo, A.; Chabinyc, M. L.; Bernstein, D. P.; Toney, M. F. *Phys. Rev. B* **2008**, *78*, 125319.

(28) Sirringhaus, H.; Brown, P. J.; Friend, R. H.; Nielsen, M. M.; Bechgaard, K.; Langeveld-Voss, B. M. W.; Spiering, A. J. H.; Janssen, R. A. J.; Meijer, E. W.; Herwig, P.; de Leeuw, D. M. *Nature* **1999**, *401*, 685.

(29) Kline, R. J.; McGehee, M. D.; Toney, M. F. *Nat. Mater.* **2006**, *5*, 222.

(30) Kim, D. H.; Park, Y. D.; Jang, Y.; Yang, H.; Kim, Y. H.; Han, J. I.; Moon, D. G.; Park, S.; Chang, T.; Chang, C.; Joo, M.; Ryu, C. Y.; Cho. K. *Adv. Funct. Mater.* **2005**, *15*, 77.

(31) Tsao, H. N.; Cho, D. M.; Park, I.; Hansen, M. R.;

Mavrinskiy, A.; Yoon, D. Y.; Graf, R.; Pisula, W.; Spiess, H. W.; Müllen, K. *J. Am. Chem. Soc.* **2011**, *133*, 2605.

(32) Zhang, W.; Smith, J.; Watkins, S. E.; Gysel, R.; McGehee, M.; Salleo, A.; Kirkpatrick, J.; Ashraf, S.; Anthopoulos, T.; Heeney, M.; McCullogh, I. *J. Am. Chem. Soc.* **2010**, *132*, 11437.

(33) Rivnay, J.; Toney, M. F.; Zheng, Y.; Kauvar, I. V.; Chen, Z.; Wagner, V.; Facchetti, A.; Salleo, A. *Adv. Mater.* **2010**, *22*, 4359.

(34) Yan, H.; Chen, Z.; Zheng, Y.; Newman, C.; Quinn, J. R.; Dötz, F.; Kastler, M.; Facchetti, A. *Nature* **2009**, *457*, 679.

(35) Rivnay, J.; Jimison, L. H.; Northrup, J. E.; Toney, M. F.; Noriega, R.; Lu, S.; Marks, T. J.; Facchetti, A.; Salleo, A. *Nat. Mater.* **2009**, *8*, 952.

(36) Rivnay, J.; Noriega, R.; Kline, R. J.; Salleo, A.; Toney, M. *Phys. Rev. B.* **2011**, *84*, 045203.

(37) Chabinyc, M. L.; W. S. Wong.; Arias, A. C.; Ready, S.; Lujan, R. A.; Daniel, J. H.; Krusor, B.; Apte, R. B.; Salleo, A.; Street, R. A. *Proc. IEEE* **2005**, *93*, 1491.

(38) McCulloch, I.; Ashraf, R. S.; Biniek, L.; Bronstein, H.; Combe, C.; Donaghey, J. E.; James, D. I.; Nielsen, C. B.; Schroeder, B. C.; Zhang, W. *Acc. Chem. Res*. **2012**, *45*, 714.

(39) Caironi, M.; Newman, C.; Moore, J. R.; Natali, D.; Yan, H.; Facchetti, A.; Sirringhaus, H. *Appl. Phys. Lett.* **2010**, *96*,

183303.

(40) Steyrleuthner, R.; Schubert M.; Jaiser, F.; Blakesley, J. C.; Chen, Z.; Facchetti, A.; Neher, D. *Adv. Mater.* **2010**, *22*, 2799.

(41) Natali, D.; Caironi, M. *Adv. Mater*. **2012**, *24*, 1357.

(42) Caironi, M.; Bird, M.; Fazzi, D.; Chen, Z.; Pietro, R. D.; Newman, C.; Facchetti, A.; Sirringhaus, H. *Adv. Funct. Mater*. **2011**, *21*, 3371.

초 록

이 논문은 높은 전자 이동도의 n형 유기 고분자 반도체를 합성하기 위해 fluorine 치환수를 달리한 fluorinated phenylene와 diketopyrrolopyrrole (DPP)을 공중합하여, fluorine 치환 개수에 따른 정공과 전자 이동도 변화에 관하여 연구한 것이다. 고분자들은 Suzuki coupling 과 Stille coupling을 통하여 고분자를 합성하였고, 그것들의 특성은 GPC, UV spectroscopy와 Cyclic voltammetry를 이용하여 분석하였다. Fluorine 개수가 증가함에 따라 각각의 고분자의 highest occupied molecular orbital (HOMO)와 lowest occupied molecular orbital (LUMO)값이 점차적으로 감소하였으며 fluorine 개수를 달리하여 측정해본 결과 fluorine 개수가 증가함에 따라 p형 반도체였던 고분자가 n형 반도체로 변하게 되면서 전자 이동도가 증가하였으며 4개의 fluorine이 치환되었을 때 가장 높은 전자 이동도 ($1.71\ cm^2V^{-1}s^{-1}$)를 보였다. 이러한 현상에 대한 원인을 알아보기 위해 2D grazing-incidence wide-angle X-ray scattering 를 이용하여 고분자의 분자 배향을 분석해본 결과, fluorine 수가 증가함에 따라서 기판에 대하여 edge-on으로 배열돼있던 고분자들이 face-on형태로 배열하게 된다는 것을 확인하여 $DPPPhF_4$의 face-on 배열은 전자 이동도를 높이는데 기여하였음을 결론지었다.

주요어: 유기트랜지스터, n 형 유기 반도체, fluorinated phenylene, diketopyrrolopyrrole

학 번: 2011-22862